Nuclear Instruments and Methods in Physics Research B

journal homepage: www.elsevier.com

Ab initio simulations on charged interstitial oxygen migration in corundum

Alexander Platonenko, Denis Gryaznov, Yuri F Zhukovskii and Eugene A Kotomin *

Institute of Solid State Physics, University of Latvia, 8 Kengaraga Str., Riga, LV-1063, Latvia

ARTICLE INFO

Article history:
Received
Received in revised form
Accepted
Available online

Keywords:
α-Al_2O_3 (corundum, sapphire)
Charged oxygen defect diffusion
Hybrid DFT-LCAO calculations

ABSTRACT

We have calculated possible migration trajectories for single-charged interstitial O_i^- anion using large-scale hybrid DFT-LCAO calculations on 2×2×1 supercells of defective α-Al_2O_3 crystals when applying *CRYSTAL14* computer code. For interstitial migration of anion, the energy barrier being calculated ~0.8-1.0 eV. Energetically most favorable configuration for charged O_i^- anion is formation of loose "dumbbell" (split interstitial) with regular O_{reg} ion. This is considerably smaller than that for neutral interstitial atoms and is in agreement with experimental data.

1. Introduction

Corundum (α-Al_2O_3, sapphire) is important radiation-resistant material with potential applications for components of diagnostic windows and breeder blankets [1–4]. Radiation-induced changes in structural and optical properties of radiation-exposed α-Al_2O_3 crystalline materials are mainly associated with aluminium and oxygen vacancies (V_{Al} and V_O) as well as complementary Frenkel pairs containing both vacancies and impurity atoms (O_i+V_O, Al_i+V_{Al}) [5–9]. The vacancies in oxygen sublattice result in the formation of electronic defects (color centers) with trapped one or two electrons electrons (the F^+ and F centers, respectively) [8–12]. It means that defects in their highest charge states are more stable under majority of conditions, however, in some cases the neutral defects can exist as well [13].

Properties of interstitial impurity atoms O_i are much less known as compared to those for electron centers, due to absence of magnetic moment and optical absorption in a suitable energy range. Recent studies reveal that in most binary oxides (as well as in alkali halides) [14,15] the anion interstitials are noticeably more mobile than complementary vacancies. Therefore, an interstitial diffusion determines the equilibrium defect concentration at elevated temperatures [16].

Ab initio calculations of O_i interstitials in different charge states have been performed so far for a number of binary metal oxides. It was predicted that interstitial oxygen atoms could form peroxide-like split interstitials (dumbbells) with the regular oxygen atoms in binary metal oxides MgO [17], α-Al_2O_3 [18,19], ZnO (wurtzite) [20], SnO_2 [21], TiO_2 (anatase) [22], CeO_2 [23,24], monoclinic HfO_2 [25] as well as in complex oxide $12CaO{\cdot}7Al_2O_3$ [26]. In most cases, the O-O distance is about 1.4–1.5 Å (table 1). Calculations performed for negatively charged oxygen interstitials reveal that it can result in an increase of the O-O distance around regular oxygen site [25,27], or interstitial oxygen can occupy empty octahedral site, where O-O distance is > 2 Å [23]. In binary metal oxides, split interstitials were observed experimentally in pure and defective SrO [28] or MgO [29] with cation vacancies, while in ZnO [30], O_i was found to be dominating acceptor responsible for loss of charge carriers upon electron irradiation.

Table 1. Bond lengths of O-O species in binary metal oxides.

Oxide	O-O distance, Å
MgO	O_2^{2-} 1.36 (1.38)[a]
Al_2O_3 (corundum)	O_2^- 1.44[b,c]
CeO_2	O_2^{2-} 1.45, O_i in octahedral position 2.36[d,e]
TiO_2 (anatase)	O_2^{2-} 1.46[f]
Monoclinic HfO_2	O_{reg}-O_i^0 1.51, O_{reg}-O_i^{1-} 2.01, O_{reg}-O_i^{2-} 2.36[g]
ZnO (wurtzite)	O_2^{2-} 1.46[h]

[a]Ref.[17],[b]Ref.[18],[c]Ref.[19],[d]Ref.[23],[e]Ref.[24],[f]Ref.[22],[g]Ref.[25],[h]Ref.[20].

Previously, we have performed hybrid DFT-LCAO calculations on the atomic and electronic structure for a neutral O_i atoms in α-Al_2O_3 using the so-called site symmetry approach [31]. For corundum, we have simulated migration trajectories of neutral O_i atoms [19] as well as atomic structures of both charged single O_i^- interstitials and dumbbells [27].

In this paper, we present the results of simulations on charged O_i^- interstitials in different configurations of defective α-Al_2O_3 bulk based of the site symmetry approach [32] and its diffusion along the different migration paths. We also estimated the activation barriers along these migration paths and have described the structural relaxation and interaction of O_i^- anion with the

* Corresponding author. e-mail: kotomin@fkf.mpg.de

nearest atoms of regular lattice. For better understanding of this defect, we also have performed a careful analysis of both calculated density of states (DOS) and vibrational frequency for the ground-state configuration. These results could help to analyze the experimental data on defect accumulation and annealing kinetics.

2. Computational details

Defective corundum crystal containing single-charged interstitial oxygen ion has been calculated using spin-polarized DFT-LCAO method with the B3PW hybrid exchange-correlation functional [33] as implemented in CRYSTAL14 package [34]. We have used the all-valence BS for atomic GTFs of oxygen (constructed using pure *s*- and *d*- as well as hybrid *sp*-AOs in the form of 6*s*-2111*sp*-1*d* as described elsewhere) [35] as well as the effective core pseudopotential (ECP) with $3s^2 3p^1$ external shell developed for aluminium [36]. For the integration within the reciprocal lattice, sampling the Brillouin zone with the 4×4×4 Monkhorst-Pack mesh realizes in order to provide a balanced summation in direct and reciprocal space of 120 atom supercell [37].

Within the SCF procedure, we have chosen the accuracies (tolerances) 7, 7, 7, 7, 14 for calculations of Coulomb and exchange integrals [34]. The SCF convergence threshold for the total electron energy has been set to either 10^{-7} a.u. for geometry optimization and total energy calculations or 10^{-9} a.u. for calculations of vibrational frequencies. The frozen phonon method (direct method) has been used [38,39]. The effective charges as well as the magnetic moments on atoms have been estimated using Mulliken population analysis [40]. In our LCAO calculations, one additional electron has been added to the O_i *sp* orbital allowing relaxation in the self-consistent calculations in order to make calculations of charged supercells, and, thus, O_i^- anions. Moreover, the difference between the numbers of spin-up and spin-down electrons has been fixed one throughout all the spin-polarized calculations. To calculate the charged supercells, a uniform background charge density has neutralized the charge in the reference cell [34]. Our selected computational scheme reproduces the bulk properties of perfect corundum very precisely, as demonstrated recently [31]. The pseudo-dumbbell solution was obtained by using the relaxed structure from the diamagnetic dumbbell configuration as initial state.

3. Results and discussion

3.1. Basic properties of O_i^- anion in corundum

We have demonstrated recently that the O_i^- defect in α-Al_2O_3 forms a "dumbbell"-like (hereafter, pseudo-dumbbell) structure [27], where the distance ($d_{O\text{-}O}$) between O_i^- and nearest regular oxygen atom (O_{reg}) is 1.87 Å. The Mulliken analysis demonstrates that both oxygen species are equivalent, *i.e.*, each atom forms three bonds with the nearest Al atoms (the corresponding O_i-Al distances equal to 1.85, 1.87 and 2.00 Å) and holds the atomic charge of -0.80 *e*. In contrast, other oxygen atoms in the supercell have four neighboring Al atoms and, consequently, larger atomic charge of ~-1 *e*. On the other hand, we have used recently the so-called site symmetry approach for defective α-Al_2O_3 crystal [31] in order to find the most stable configuration for the neutral O_i interstitial. We have demonstrated in that study the formation of well-known diamagnetic dumbbell configuration. In the present study, we use the site symmetry approach for the charged O_i^- defects in corundum to deeper discuss possible differences between both kinds of dumbbells and to compare their properties.

The site symmetry approach gives a number of possible defect configurations depending on the defect's position regarding to Wyckoff positions in crystal lattice and its splitting in the supercell model. In our calculations the defective crystal represented the 121 atoms supercell with the space group P3- due to inserting O_i in the Wyckoff position 2*b* (vacant Wyckoff position with the coordinates (0,0,0) in the primitive unit cell). As shown in Ref. 31, the splitting of Wyckoff position 2*b* leads to the following site symmetries: *S*1(6*g*), *S*2(3*e*), *S*3(2*d*), *S*6(1*a*), where SP denotes the site symmetry point group with P point symmetry operations. The site symmetry approach suggested several solutions for the neutral [31] and charged oxygen interstitial defects. The calculated solutions are distinguished by the interatomic distances (*d*), the atomic charges (*q*) and the O_i magnetic moments (*μ*). Also, the analysis of DOS revealed important information on such defects.

As expected, due to electrostatic interactions between the charged O_i and neighboring Al_{reg} lattice atoms, the distance between O_i and O_{reg} atom is always larger than for neutral oxygen interstitial independently of the solution obtained. Nevertheless, in the most stable configuration, $d_{O\text{-}O}$ = 1.87 Å. In this case, the atomic charges and magnetic moments of both oxygens are the same, *i.e.*, 0.79 *e* and 0.49 μ_B, respectively. Because of such a symmetrical behavior, we call this a pseudo-dumbbell. Other configurations, in the site symmetry approach, show larger $d_{O\text{-}O}$ (table 2 for *S*1 and *S*3 sites) and less favorable in energy: 0.55 eV for *S*1 and 1.33 eV for *S*3. Notice that the solutions for *S*1 and *S*2 as well as for *S*3 and *S*6 are identical and, thus, are not present in table 2. The increased values of $d_{O\text{-}O}$ correlate with the slightly smaller q_{Oi} as compared to the pseudo-dumbbell. It means also that O_{reg} should have the atomic charges (-0.95 and -0.96 *e*) which are very close to those for other host oxygens in the supercell. Consequently, μ_{Oreg} (0.10 μ_B for *S*1 and 0.05 μ_B for *S*3) decrease whereas μ_{Oi} increase (0.81 μ_B for *S*1 and 0.76 μ_B for *S*3).

Table 2 Results obtained for O_i^- atom placed in four different split vacant positions and pseudo-dumbbell configuration. 1NN and 2NN denote first and second nearest neighbours, *q* and *μ* atomic charge and magnetic moment (in *e* and μ_B, respectively). Mulliken bond populations (*e*) are given for the interaction between O_i and nearest O_{reg} only.

Position	Pseudo-dumbbell	*S*1 (*S*2)	*S*3 (*S*6)
Point Symmetry	*C*1	*C*1	*C*3
1NN Distance $d_{O\text{-}Al}$, Å	2 Al 1.85 1.87	2 Al 1.80	2 Al 1.80
2NN Distance $d_{O\text{-}O}$, Å	O 1.87	2O 2.14	6O 2.22
Bond population O_i-O_{reg}, e	-0.14	-0.06	-0.02
q_{Oi}/μ_{Oi}	-0.79/0.49	-0.58/0.81	-0.61/0.76
q_{Oreg}/μ_{Oreg}	-0.79/0.49	-0.95/0.10	-0.96/0.05

3.2. O_i^- migration paths and barriers energy

The stable pseudo-dumbbell configuration in corundum supercell discussed above is a starting point for simulation on migration paths (Fig. 1). Migration path calculations were performed by freezing O_i coordinates and fully optimising geometry of the rest supercell. Then, the distance between O_i and

the host oxygen atom (O_{reg}) was changed in the initial configuration and procedure recurs. We performed calculations on 10 points for each trajectory. In the last point of each trajectory, we performed optimization without coordinate freezing, to obtain lowest energy solution. If the final dumbbell configuration in last point was the same as at the starting point, the migration path considered valid. We assume that O_i^- and vacancy are enough separated which does not affect O_i^- migration.

Fig. 1 presents seven possible migration paths towards the nearest regular oxygen atoms, with distances ranging from 2.18 Å to 3.11 Å. Three trajectories (2.52 Å, 2.64 Å and 3.11 Å) lie very closely to high-symmetrical octahedral position. Thus we consider paths are V-VII very similar to those described in our previous paper [27], where the energy barrier for migration through centre of octahedra was estimated as 0.76 eV. Therefore, they are not discussed here in details.

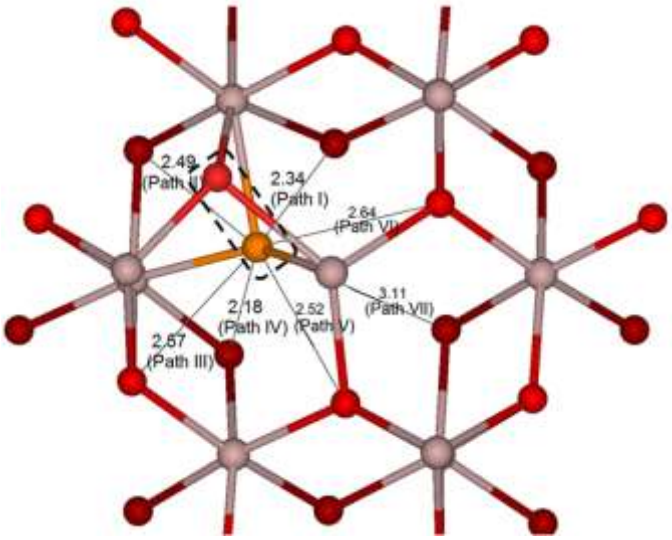

Figure 1. Atop view of seven possible migration paths for O_i^- atom (shown as orange ball). Gray-brown balls correspond to Al atoms, while light and dark red atoms correspond to O atoms in different planes. Pseudo-dumbbell is shown as a dashed rectangle

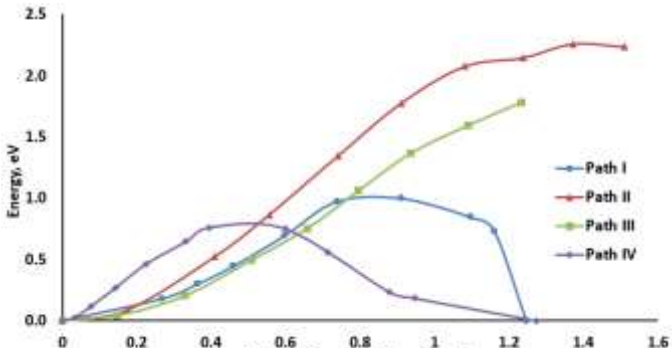

Figure 2. The energy curves for four migration paths of interstitial O_i^- atom with the estimated energy barriers.

The energy curves for four new O_i^- migration paths are shown in Fig. 2: two of them (I and IV) reveal energy barrier and end up by forming new dumbbell with a host oxygen atom; whereas two others (II and III) show only energy rise along the O_i^- displacement. To interpret these results, let took a closer look on O_i^- surrounding along each path. Table 3 shows O_i surrounding at

Table 3 O_i^- configurations at the top of energy barriers along the migration trajectories (Fig. 2). NN denotes nearest neighbors.

Trajectory	I	II	III	IV
Energy barrier, eV	1.0	>2.26	>1.78	0.76
NN Distance, Å	Al 1.76 O 1.87 Al 1.89 Al 2.11	Al 1.66 Al 1.71 O 1.83 O 2.14	Al 1.72 Al 1.90 Al 1.93 O 1.94 O 1.98	Al 1.85 O 1.92 O 1.95 Al 1.98
Bond population of O_i with NN	0.346 -0.147 0.324 0.234	0.506 0.444 -0.149 -0.089	0.466 0.252 0.226 -0.098 -0.084	0.298 -0.159 -0.146 0.240

maximum energy point. The lowest estimated I and IV barriers for migration are 0.8-1.0 eV. Obviously, maximum impact on the energy gain along the paths have the nearest Al atoms. While paths with minimal barriers lie near octahedral site, trajectories with higher energy go through tetrahedral sites, where O_i^- becomes very close to Al atoms and this results in formation of Al-O bonds, which make further diffusion impossible. Similar behaviour was observed in our previous calculations [27], where the migration barrier was determined by Al-O bond breaking and switching. Trajectories I and IV with smaller starting O_i-O_{reg} distance (Fig. 1) show energy barrier for migration. While II and III had energy higher for 0.7-1.2 eV after displacing O_i atom for more than 1.2 Å from initial position. Thus, those trajectories were considered unsuitable for further calculations. Semi-covalent bonding observed in corundum experimentally [41], characterized by oxygen atomic charge -0.9 *e*. Therefore, in the case of a neutral O_i stronger O_i-O_{reg} interaction occurs due to charge redistribution, where O_i acts as an electron acceptor. For charged interstitial atomic charge is similar to regular oxygen atoms (0.79 *e vs.* 0.99 *e*) with charge of 0.2 *e* transferred towards Al atoms.

3.3. Electronic structure of pseudo-dumbbell configuration

The calculated projected DOS for the calculations of pseudo-dumbbell and position of O_i^- at *S*1 and *S*3 (Fig. 3). As known, in α-Al_2O_3 the valence band consists of O 2*p* electrons whereas the Al electrons contribute mainly to the conduction band. The changes due the presence of O_i^- are seen from additional defect bands in the band gap, and their position depends on the structure configuration obtained. The two peaks seen for spin-up (at ~-1.5 and 0 eV) and spin-down (at -2 and -1 eV) electrons before the Fermi energy in fig. 3a (pseudo-dumbbell) are due to fully occupied p_x and p_y orbitals and partly occupied p_z orbital. One of these peaks in the spin-up state, namely at 0 eV, corresponds to the unpaired electron occupying the p_z orbital. The energy splitting between *p* orbitals as seen in fig. 3a below the Fermi energy makes the difference in the behavior of neutral dumbbell and charged O_i (pseudo-dumbbell) defects in α-Al_2O_3 (see our calculated DOS for neutral dumbbell O_i in ref. 31). The observed difference in the behaviour of these two defects is to large extent explained by larger $d_{O\text{-}O}$ in the case of charged defect (1.44 vs 1.87 Å). Since the p_z orbital of O_i is only partly occupied, there appears one more additional peak above the Fermi energy.

The qualitative picture for the *S*1-position (fig. 3b) is very similar. The energy splitting effect as discussed for the pseudo-dumbbell defect is also seen in fig. 3b. However, the band due to the additional electron in the spin-down state lies at the Fermi energy. So, the molecular orbitals are filled in very similar manner in the cases of pseudo-dumbbell defect and *S*1 position.

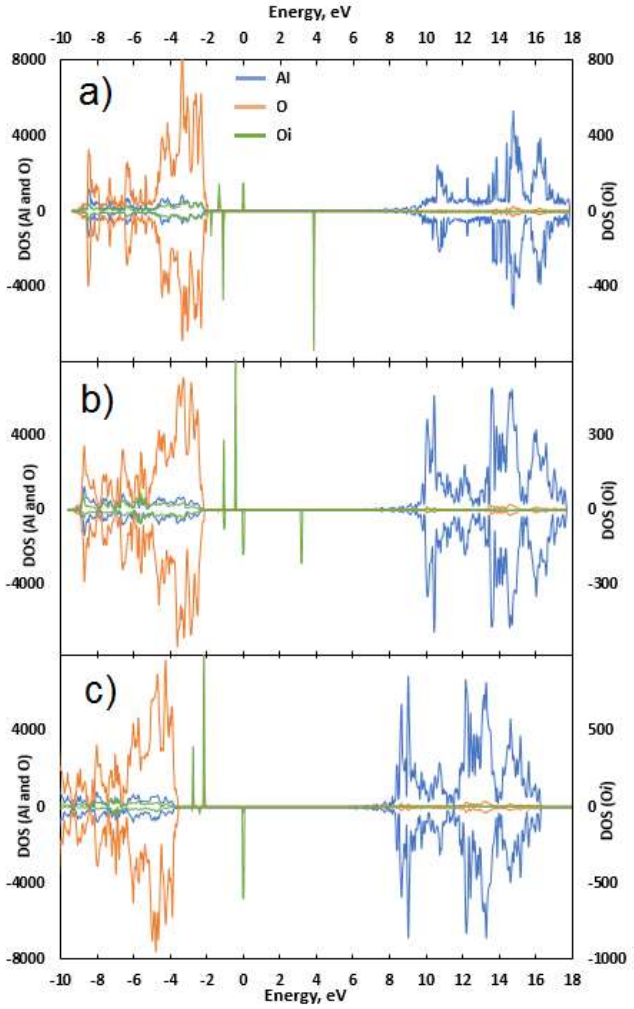

Figure 3. Density of states (DOS) for calculations of pseudo-dumbbell O_i configuration (a), *S*1 (b) and *S*3 (c). Negative values correspond to spin down electrons. The Fermi energy is taken as zero. O_i DOS corresponds to right *y*-axis

Here the bond population analysis is quite informative, too, and helps to deeper understand the behavior of O_i^- in different configurations. It reveals a negative value of -0.14 *e* for the interaction of O_i^- and O_{reg} atoms but positive values of 0.30 *e* and 0.32 *e* for the interaction of O_i^- and the two neighboring Al atoms (table 2) in the pseudo-dumbbell configuration. Such values of bond population are consistent with the equal magnetic moment and atomic charge on O_i and O_{reg}. In contrast, the *S*1- and *S*3 positions for O_i^- are characterized by lower negative values of the bond population for the interactions of O_i^- with O_{reg} atoms. The negative values of bond population (table 2) could demonstrate the trend of instability of O_i^- at *S*1 and *S*3 positions.

On the basis of present DOS and Mulliken population analysis we could suggest that the full description and characterization of charged or neutral O_i in α-Al_2O_3 should be based on the energetic parameter like the formation energy, the structure parameter like the distance between O_i and O_{reg}, electronic structure with the help of DOS, and bond population.

Calculated vibrational frequencies for pseudo-dumbbell configuration do not show common vibration between O_i^- and O_{reg}. However, there are two vibrational frequencies around 877 and 937 cm^{-1} formed by bending and stretching of Al and O bonds, which are involved in pseudo-dumbbell formation. While in case of neutral O_i, O_i-O_{reg} had vibrational frequency of 1067 cm^{-1}, which is typical for peroxides O_2^{2-} [31].

4. Conclusions

The estimated lowest energy barrier for migration of neutral O_i is ~1.3 eV [19]. In partly covalent corundum the regular oxygen atomic charge is -0.9 *e* [41]. Therefore, in the case of a neutral O_i stronger O_i-O_{reg} interaction occurs due to charge redistribution within a dumbbell. Instead, for a charged interstitial the atomic charge is similar to a regular oxygen atoms (-0.79e vs. -0.99e) and thus charge is redistributed more towards Al atoms without making a strong chemical O-O bond. This explains absence of the vibrational frequencies within a pseudo-dumbbell. Its migration energy 0.8-1.0 eV is noticeably smaller than for a neutral interstitial, in agreement with the experimental data [42].

Acknowledgements

We have performed this work within the framework of the EUROfusion Consortium receiving funding from the European grant agreement 633053. The views and opinions expressed herein do not necessarily reflect those of the European Commission. Authors thank R. Vila, A.I. Popov, A. Luchshik and R.A. Evarestov for fruitful discussions. To carry out large-scale calculations, we have used the HPC supercomputer at Stuttgart University (Germany)

References

1. J. H. Crawford, Defects and defect processes in ionic oxides: Where do we stand today? Nucl. Inst. Methods Phys. Res. B 108 (1984) 159–165.
2. J. Valbis, N. Itoh, Electronic excitations, luminescence and lattice defect formation in α-Al_2O_3 crystals. Radiat. Eff. Defects Solids 116 (1991) 171–189.
3. F. Mota, C.J. Ortiz, R. Vila, N. Casal, A. Garcia, A. Ibarra, Calculation of damage function of Al_2O_3 in irradiation facilities for fusion reactor applications. J. Nucl. Mater. 442 (Suppl. 1) (2013) 5699-5704.
4. A. Serikov, L. Bertalot, M. Clough, U. Fischer, A. Suarez, Neutronics analysis for ITER cable looms. Fusion Eng. Des. 96–97 (2015) 943–947.
5. B.D. Evans, A review of the optical properties of anion lattice vacancies, and electrical conduction in α-Al_2O_3: Their relation to radiation-induced electrical degradation. J. Nucl. Mater. 219 (1995) 202–223.
6. R.S. Averback, P. Ehrhart, A.I. Popov, A. von Sambeek, Defects in ion implanted and electron irradiated MgO and Al_2O_3. Radiat. Eff. Defects Solids 136 (1995) 169–173.
7. E.A. Kotomin, A.I. Popov, A. Stashans, A novel model for F^+ to *F* photoconversion in corundum crystals. J. Phys.: Condens. Matt. 6, (1994) L569–L573.
8. J. Carrasco, N. Lopez, C. Sousa, F. Illas, First-principles study of the optical transitions of *F* centers in the bulk and on the (0001) surface of α-Al_2O_3. Phys. Rev. B 72 (2005) 054109 (1-9).
9. C.S. Praveen, V. Timon, M. Valant, Electronic band gaps of ternary corundum solid solutions from Fe_2O_3–Cr_2O_3–Al_2O_3 system for photocatalytic applications: A theoretical study. Comput. Mater. Sci. 55 (2012) 192–198.
10. E.A. Kotomin, A.I. Popov, Radiation-induced point defects in simple oxides. Nucl. Instrum. Methods Phys. Res. B 141 (1998)

1–15.

11. E.A. Kotomin, A.I. Popov, A. Stashans, Computer modelling of radiation damage in cation sublattice of corundum. Phys. Status Solidi B 207 (1998) 69–73.
12. A. Lushchik, Ch. Lushchik, K. Schwartz, E. Vasil'chenko, T. Kärner, I. Kudryavtseva, V. Issakhanyan, A. Shugai, Stabilization and annealing of interstitials formed by radiation in binary metal oxides and fluorides. Nucl. Instrum. Methods Phys. Res. B 266 (2008) 2868–2871.
13. N.D.M. Hine, K. Frensch, W.M.C. Foulkes, M.W. Finnis, Supercell size scaling of density functional theory formation energies of charged defects. Phys. Rev. B 79 (2009) 024112 (1–13).
14. A.L. Shluger, V.E. Puchin, T. Suzuki, K. Tanimura, N. Itoh, Optical transitions of the *H* centers in alkali halides. Phys. Rev. B 52 (1995) 4017–4028.
15. J. Maeda, T. Okada, Theoretical study of optical transitions of *H* centers in potassium halides. J. Lumin. 87 (2000) 564–567.
16. E.A. Kotomin, V.N. Kuzovkov, A.I. Popov, M.A. Monge, R. González, Y. Chen, Diffusion-controlled annihilation and aggregation of *F*-centers in thermochemically reduced MgO crystals. Nucl. Instrum. Methods Phys. Res. B 191 (2002) 208–211.
17. T. Brudevoll, E.A. Kotomin, N.E. Christensen, Interstitial-oxygen-atom diffusion in MgO. Phys. Rev. B 53 (1996) 7731–7735.
18. A.A. Sokol, A. Walsh, C.R.A. Catlow, Oxygen interstitial structures in close-packed metal oxides. Chem. Phys. Lett. 492 (2010) 44–48.
19. Yu.F. Zhukovskii, A. Platonenko, S. Piskunov, E.A. Kotomin, *Ab initio* simulations on migration paths of interstitial oxygen in corundum. *Nucl. Instrum. Methods Phys. Res. B* 374 (2016) 29-34.
20. S. Limpijumnong, X. Li, S.H. Wei, S.B. Zhang, Substitutional diatomic molecules NO, NC, CO, N_2, and O_2: Their vibrational frequencies and effects on *p* doping of ZnO. Appl. Phys. Lett. 86 (2005) 1–3.
21. K.G. Godinho, A. Walsh, G.W. Watson, Energetic and electronic structure analysis of intrinsic defects in SnO_2. J. Phys. Chem. C 113 (2009) 439–448.
22. S. Na-Phattalung, M.F. Smith, K. Kim, M.H. Du, S.H. Wei, S.B. Zhang, S. Limpijumnong, First-principles study of native defects in anatase TiO_2. Phys. Rev. B **73** 1–6 (2006).
23. T. Zacherle, A. Schriever, R.A. De Souza, M. Martin, Ab initio analysis of the defect structure of ceria. Phys. Rev. B 87 (2013) 1–11.
24. P.R.L. Keating, D.O. Scanlon, B.J. Morgan, N.M. Galea, G.W. Watson, Analysis of intrinsic defects in CeO_2 using a Koopmans-like GGA+*U* approach. J. Phys. Chem. C **116,** 2443–2452 (2012).
25. A.S. Foster, F. Lopez Gejo, A.L. Shluger, R.M. Nieminen, Vacancy and interstitial defects in hafnia. Phys. Rev. B 65 (2002) 174117 (1–3).
26. K. Kajihara, S. Matsuishi, K. Hayashi, M. Hirano, H. Hosono. Vibrational dynamics and oxygen diffusion in a nanoporous oxide ion conductor $12CaO{\cdot}7Al_2O_3$ studied by ^{18}O labeling and micro-Raman spectroscopy. J. Phys. Chem. C 111 (2007) 14855–14861.
27. A. Platonenko, D. Gryaznov, S. Piskunov, Yu.F. Zhukovskii, E.A. Kotomin, Charged oxygen interstitials in corundum: First principles simulations. Phys. Status Solidi C 13 (2016) 932–936.
28. V. Seeman, S. Reifman, T. Lehto, Ü. Haldre, Family of O_2^- centres in SrO crystals. Phys. Status Solidi B **459** (1980) 459–465.
29. A. Lushchik, T. Kärner, Ch. Lushchik, E. Vasilchenko, S. Dolgov, V. Isakhanyan, P. Liblik, Dependence of long-lived defect creation on excitation density in MgO single crystals. Phys. Status Solidi C 4 (2007) 1084–1087.
30. K.E. Knutsen, A. Galeckas, A. Zubiaga, F. Tuomisto, G.C. Farlow, B.G. Svensson, A.Yu. Kuznetsov, Zinc vacancy and oxygen interstitial in ZnO revealed by sequential annealing and electron irradiation. Phys. Rev. B 86 (2012) 121203(1–5).
31. R.A. Evarestov, A. Platonenko, D. Gryaznov, Yu.F. Zhukovskii, E.A. Kotomin, First-principles calculations of oxygen interstitials in corundum: site symmetry approach. Phys. Chem. Chem. Phys. Commun. (2017) *submitted*.
32. R.A. Evarestov, Yu.E. Kitaev, V.V. Porsev, Use of Wyckoff position splittings in the supercell model of crystals with point defects. J. Appl. Crystallogr. 50 (2017) 893–900.
33. A.D. Becke, Density-functional thermochemistry. III. The role of exact exchange. J. Chem. Phys. 98 (1993) 5648–5652.
34. R. Dovesi, V.R. Saunders, C. Roetti, R. Orlando, C.M. Zicovich-Wilson, F. Pascale, B. Civalleri, K. Doll, N.M. Harrison, I.J. Bush, Ph. D'Arco, M. Llunell, M. Causà, Y. Noël, CRYSTAL14 User's Manual (University of Torino, 2014).
35. J. Baima, A. Erba, M. Rérat, R. Orlando, R. Dovesi, Beryllium oxide nanotubes and their connection to the flat monolayer. J. Phys. Chem. C 117 (2013) 12864–12872.
36. M. Causà, R. Dovesi, C. Roetti, Pseudopotential Hartree-Fock study of seventeen III-V and IV-IV semiconductors. Phys. Rev. B 43 (1991) 11937–11943.
37. H.J. Monkhorst, J.D. Pack, Special points for Brillouin-zone integrations. Phys. Rev. B 13 (1976) 5188–5192.
38. F. Pascale, C.M. Zicovich-Wilson, F. López Gejo, B. Civalleri, R. Orlando, R. Dovesi The calculation of the vibrational frequencies of crystalline compounds and its implementation in the CRYSTAL code. J. Comput. Chem. 25 (2004) 888–897.
39. C.M. Zicovich-Wilson, F. Pascale, C. Roetti, V.R. Saunders, R. Orlando, R. Dovesi, Calculation of the vibration frequencies of α-quartz: The effect of Hamiltonian and basis set. J. Comput. Chem. 25 (2004) 1873–1881.
40. R.S. Mulliken, Electronic population analysis on LCAO–MO molecular wave functions. J. Chem. Phys. 23 (1955) 1833–1840.
41. J. Lewis, D. Schwarzenbach, H.D. Flack, Electric field gradients and charge density in corundum, α-Al_2O_3. Acta Crystallogr. *A* 38 (1982) 733–739.
42. E.A. Kotomin, V.N. Kuzovkov, A.I. Popov, R. Vila, Kinetics of the *F* center annealing and colloid formation in Al_2O_3. Nucl. . Instrum. Methods Phys. Res. B 374 (2016) 107-110.

Institute of Solid State Physics, University of Latvia as the Center of Excellence has received funding from the European Union's Horizon 2020 Framework Programme H2020-WIDESPREAD-01-2016-2017-TeamingPhase2 under grant agreement No. 739508, project CAMART²